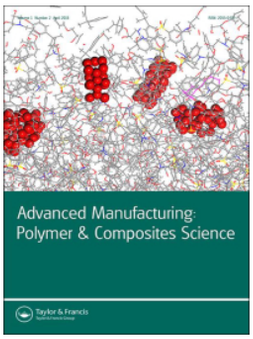

Taylor & Francis
Taylor & Francis Group

Advanced Manufacturing: Polymer & Composites Science

ISSN: (Print) (Online) Journal homepage: www.tandfonline.com/journals/yadm20

Influence of manufacturing-induced defects on the fatigue performances of autoclave moulded laminates

L. Maragoni, P. A. Carraro & M. Quaresimin

To cite this article: L. Maragoni, P. A. Carraro & M. Quaresimin (2021) Influence of manufacturing-induced defects on the fatigue performances of autoclave moulded laminates, Advanced Manufacturing: Polymer & Composites Science, 7:2, 36-47, DOI: 10.1080/20550340.2021.1967650

To link to this article: https://doi.org/10.1080/20550340.2021.1967650

ADVANCED MANUFACTURING: POLYMER & COMPOSITES SCIENCE
2021, VOL. 7, NO. 2, 36–47
https://doi.org/10.1080/20550340.2021.1967650

Influence of manufacturing-induced defects on the fatigue performances of autoclave moulded laminates

L. Maragoni, P. A. Carraro and M. Quaresimin

Department of Management and Engineering, University of Padova, Vicenza, Italy

ABSTRACT

In the present work, cross-ply and multidirectional laminates were produced by autoclave moulding. Changes in the process parameters led to different microstructural features in terms of fibre volume fraction, global void content, and void size. Fatigue tests revealed a strong influence of the microstructure on the long-term performances of the laminates, in terms of life to crack initiation, crack propagation, crack density evolution and associated stiffness drop. A criterion recently proposed by the authors to predict the formation of the first fatigue cracks accounting for the actual material microstructure, including voids, was then validated on the new experimental data. The results show the need to properly account for the manufacturing induced defects for a more efficient and safer design of composite parts, and remark the necessity of developing models that link manufacturing process parameters, micro-scale morphology, and mechanical performances to enable a cost-effective production that maximizes the performance/cost ratio.

GRAPHICAL ABSTRACT

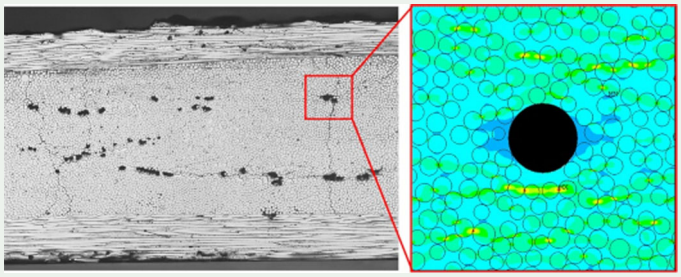

KEYWORDS

Fatigue; damage evolution; crack; defects; voids; autoclave

1. Introduction

The manufacturing process for composite parts inevitably leads to microstructural defects, such as irregular fibre distribution, non-homogeneous fibre volume fraction, and the presence of porosity. Manufacturing-induced defects, and in particular voids, have been shown to deeply affect the mechanical response of composite laminates, both under static and cyclic loadings (see, among others, [1–19]). In particular, voids were found to significantly affect the fatigue behaviour by reducing the life to crack initiation, increasing the crack growth rate, and promoting the final separation of the laminates. In the last years, the authors devoted large efforts in characterising and modelling the effect of voids on the mechanical response of composites and, in particular, on their fatigue behaviour [14,17,18,20]. The reader is referred to those works, as well as to Mehdikhani et al. [21] for more extensive literature reviews on the subject.

In [18] an extensive experimental campaign was carried out on glass/epoxy laminates with different stacking sequences made with vacuum resin infusion cured at room temperature (i.e.: without thermal stresses), highlighting a large effect of voids on the fatigue damage initiation and evolution. Those experimental data were then used to validate a criterion to predict the life to crack initiation in the presence of uniformly distributed micro-voids [20].

Within this framework, the objective of the present work is twofold. First, to observe quantitatively if the effect on the mechanical response of microstructural defects produced by a different manufacturing process is comparable to that found in [18], contributing to a more comprehensive overall

CONTACT M. Quaresimin marino.quaresimin@unipd.it Department of Management and Engineering, University of Padova, Stradella San Nicola 3, Vicenza, Italy

Supplemental data for this article is available online at https://doi.org/10.1080/20550340.2021.1967650.

Table 1. Process parameters of the produced laminates.

Laminate	Lay-up	Curing temperature (°C)	Curing pressure (bar)	Vacuum (bar)	Curing time (hours)	Layers of breather (300g/m^2)	Perforated release film
CP1	$[0/90_2]_S$	125	5	−1	1	2	No
CP2	$[0/90_2]_S$	125	5	−1	1	2	Yes
CP3	$[0/90_2]_S$	125	7	−1	1	2	Yes
MD1	$[0/50_2/0/\text{-}50_2]_S$	100	7	−1	3	2	Yes
MD2	$[0/50_2/0/\text{-}50_2]_S$	100	1	0	3	2	Yes

characterisation of the effect of voids on the long-term behaviour of composites and providing a reference for the choice of the optimal manufacturing process for a given part.

The second purpose of this work is to further validate the predictive model proposed in [20], in order to assess its general validity. Indeed, the model was validated only for uniformly distributed voids in laminates having approximately the same fibre volume fraction. In practice, the fibre volume fraction, the void shape distribution and the void spatial configuration can vary as a function of the manufacturing process, so that a predictive model must be capable of taking such changes into account.

Autoclave moulding was chosen as the manufacturing process for the present experimental campaign. Indeed, despite the interest towards less expensive out-of-autoclave solutions (such as RTM and vacuum infusion), and the introduction of new technologies (like additive manufacturing), the autoclave process is still widely used as it allows to obtain the best material performances and, being it a well-known process, prevents the issues related to the introduction of new technologies in fields where strict certifications are needed. Despite it being a well-established process, an in-depth quantitative analysis of the effect of the microstructure on the fatigue performance is currently missing in the open literature. As previously mentioned, with respect to the laminates produced by vacuum infusion of Maragoni et al. [18], the autoclave process could lead to different microstructural features. In addition, it also induces thermal stresses in the moulded laminate, which must properly be accounted for.

Both cross-ply (CP) and multidirectional (MD) laminates were produced varying the process parameters, so that different combinations of fibre volume fraction and void content were obtained. The microstructure was characterised and quantified in detail by micrographic observations. The influence of microstructure on the fatigue performances was investigated in terms of life to first cracks initiation, crack growth rate, crack density evolution and stiffness decrease during the fatigue life. Finally, a criterion recently developed by the authors to predict the first cracks initiation taking the actual microstructure into account [20] is applied to the new experimental data.

2. Materials and testing

In this section, a thorough description is given of the laminates manufacturing, the morphological characterisation, and the testing techniques.

2.1. Laminates manufacturing

According to Carraro and Quaresimin [22] and Quaresimin et al. [23], the crack initiation process under cyclic loadings is driven by different parameters depending on the shear to transverse stress ratio $\lambda_{12} = \sigma_6/\sigma_2$ acting in an off-axis ply. Such driving forces were identified as the Local Hydrostatic Stress (LHS, for $\lambda_{12} < \lambda_{12}^* \approx 0.5$) and the Local Maximum Principal Stress (LMPS, for $\lambda_{12} > \lambda_{12}^* \approx 0.5$). Thus, in the present work two sets of laminates were produced by autoclave moulding, to analyse their fatigue behaviour under both LHS- and LMPS-dominated conditions. The first set was characterised by a $[0/90_2]_S$ stacking sequence (LHS-dominated), whereas the second by a $[0/50_2/0/\text{-}50_2]_S$ lay-up (LMPS-dominated).

A glass/epoxy pre-preg UE400-REM (CIT, Italy) was used to produce all the laminates. The glass/epoxy system was chosen as its transparency allows an easy and precise quantification of the damage evolution with the aid of a back-light illumination system [18, 24].

Three $[0/90_2]_S$ and two $[0/50_2/0/\text{-}50_2]_S$ laminates were produced. Laminates with the former and latter lay-ups will be from now on referred to as CP (Cross-ply) and MD (Multidirectional), respectively. The process parameters used in all cases are reported in Table 1, and the temperature and pressure profiles are shown in Figure 1 along with a schematization of the manufacturing lay-up. For panel CP1, a non-perforated release ply was used, thus keeping the fibre volume fraction V_f of the raw pre-preg. Given the low value of such a volume fraction compared to most of the structural composite applications (see Section 2.2), it was decided to produce the laminate CP2 with a perforated release ply that allowed the breather layers placed above it to absorb part of the resin, while keeping a cure pressure of 5 bar. To proceed further in the same direction, panel CP3 was produced with a perforated release ply and increasing the curing pressure from 5 to 7 bars. As shown in the next section, the increase in pressure combined with the use of a

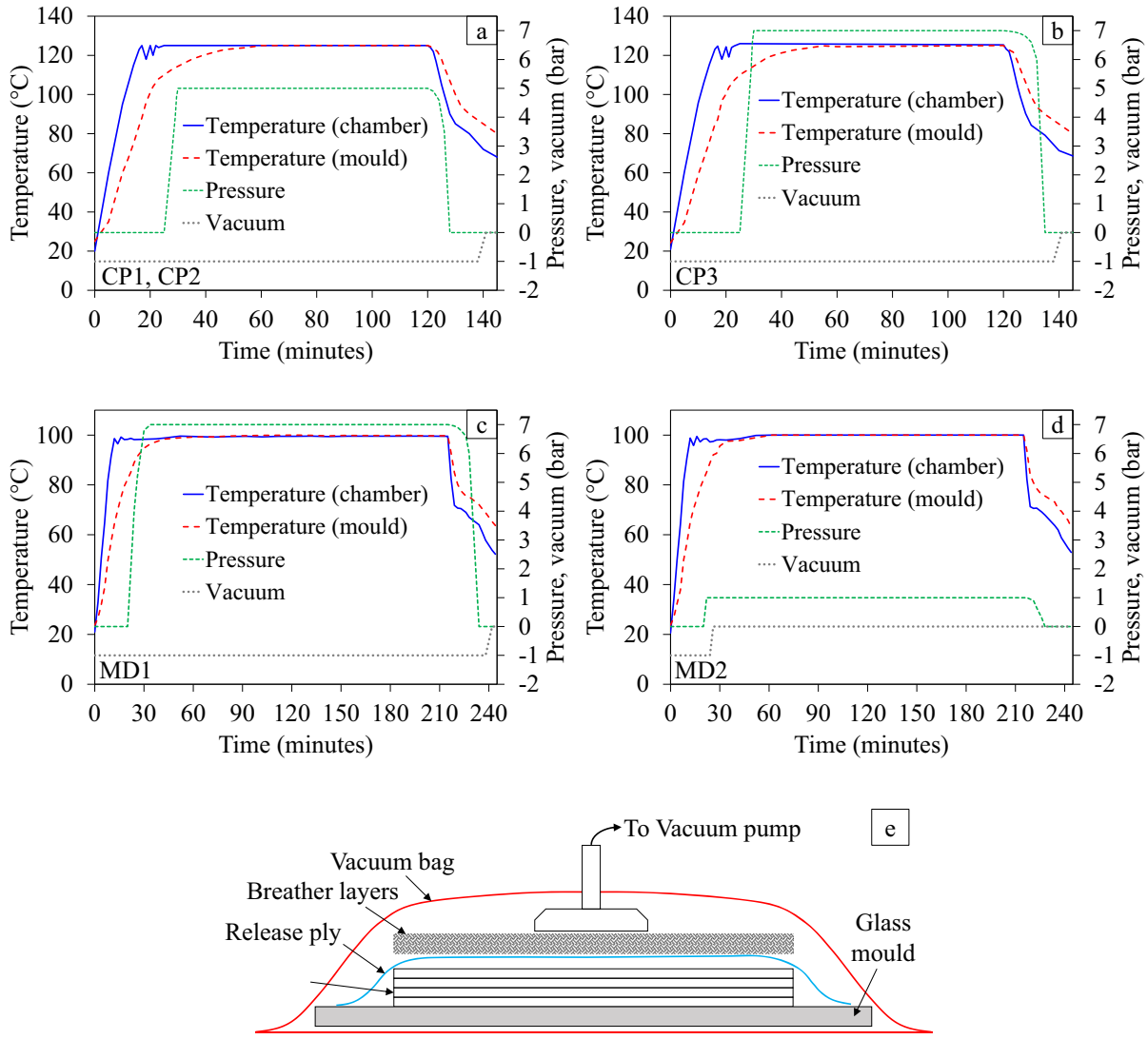

Figure 1. Temperature and pressure profiles for laminates a) CP1 and CP2, b) CP3, c) MD1, d) MD2, and e) schematization of manufacturing lay-up.

perforated release ply led to a larger V_f but also caused an increase in void content due to an excessive resin loss. The curing temperature for all the CP laminates was 125 °C, as recommended by the pre-preg supplier. As discussed in Section 2.2, different process parameters led to different fibre volume fractions and void contents in the CP laminates.

The parameters used to produce the MD laminates were chosen to have a fibre volume fraction as similar as possible (around 0.5) with, respectively, a low and a high void content. For those laminates, the combination of a perforated release ply and a curing temperature of 125 °C was found to lead to an excessive resin loss, not allowing to obtain a laminate with a low void-content. Therefore, a curing temperature of 100 °C was used, increasing the curing time to three hours to guarantee a complete cure of the resin. The curing time and pressures for MD laminates reported in Table 1 are those that lead to the desired microstructural results (see section 2.2).

All the produced panels had a size of 300 mm x 200 mm, and the final total thicknesses were 2.158 mm (CP1), 1.469 mm (CP2), 1.432 mm (CP3), 3.275 mm (MD1), and 3.553 mm (MD2). After the cure was complete, specimens with a width of about 22 mm were cut with a circular saw, and their edges polished down to a 0.5 μm SiO_2 suspension to prevent premature crack initiation at the edges and to allow precise micrographic observations.

2.2. Microstructural characterisation

The microstructure of the produced laminates was characterised by the fibre volume fraction V_f and the void content, both calculated in the off-axis plies.

The fibre volume fraction was estimated from micrographic images taken on five dedicated

samples cut from the produced panels. The observation plane was perpendicular to the fibre direction, implying additional cuts for the off-axis angles at ±50°. To increase the contrast between glass fibre and resin, the specimen edges were etched with concentrated H_2SO_4 (96%), 20 s for three times. Fibres were detected with an in-house developed tool that uses a Matlab® built-in algorithm based on the Hough transform. The average fibre diameter resulted to be 15.51 μm. Ten images at 200x for each sample were analysed, and the resulting V_f values are reported in Table 2.

The void content was estimated from micrographs taken on all the tested samples, scanning the full length of the observation area (see section 2.3) on both the specimen edges, for a total of 60 micrographs per sample with a magnification of 100x. Representative pictures of all the CP and MD laminates are shown in Figure 2. Voids were found to be uniformly distributed along the specimen length for all the laminates. For laminate CP1, in addition to voids of size a few times that of the fibres, also few very large, flattened voids were present (Figure 2(b)). The void content was quantified by both the void area fraction (A_v) and the average void equivalent diameter ($D_{v,av}$), defined as the diameter of a circle having the same area of the actual transverse void section. This is a 2 D quantification of the void content and size which the authors believe to be representative of the material microstructure due to the cigar-like shape of the voids, which were elongated along the fibre direction. This configuration is typical for UD plies [21] and was observed also for infused laminates [18]. In addition, the majority of voids were found to have a roughly round section, and only in few cases, namely in laminates CP1 and MD2, some of them were flattened. Void detection from the micrographs was carried out using an in-house built Matlab® code based on greyscale image

Table 2. Microstructural features of the produced laminates.

Laminate	V_f (%)	A_v (%)	$D_{v,av}$ (μm)
CP1	38.8	0.62	98.46
CP2	58.8	0.73	54.48
CP3	61.3	1.48	38.07
MD1	53.0	0.37	65.64
MD2	47.2	4.20	108.63

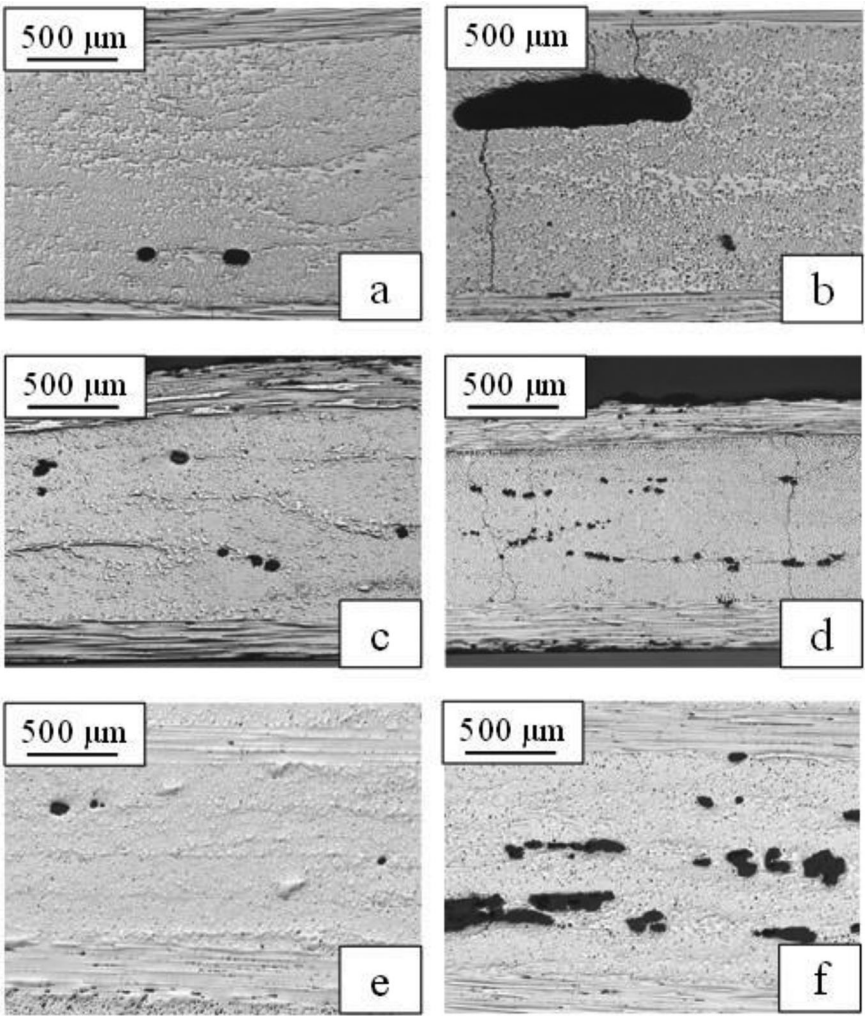

Figure 2. Representative micrographs of laminates (a,b) CP1, (c) CP2, (d) CP3, (e) MD1, and (f) MD2.

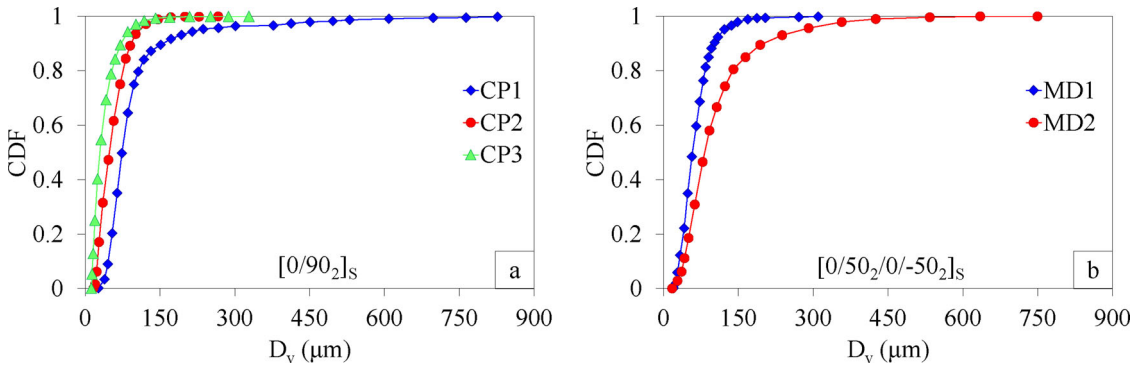

Figure 3. Cumulative Distribution Function (CDF) of the void equivalent diameter (D_v) of the produced (a) cross ply (CP), and (b) multidirectional (MD) laminates.

binarization, exploiting the darker colour of the voids compared to resin and fibre.

The resulting A_v and $D_{v,av}$ are reported in Table 2. In Figure 3, the Cumulative Distribution Function (CDF) of the void equivalent diameter D_v is shown for all the laminates. It is possible to observe the presence of the few very large, flattened voids in laminate CP1 that characterise the highest part of the curve. For MD laminates, the void content and features were found to be very similar in the $+50°$ and $-50°$ ply, hence a single value of A_v and $D_{v,av}$ is reported in Table 2.

2.3. Testing methods

Before testing, glass/epoxy tabs were bonded to the specimens. Fatigue tests were carried out with a MTS858-Minibionix servo hydraulic testing machine, equipped with a 25 kN load cell.

The tests were conducted in load control, with a load ratio (minimum to maximum applied load ratio) $R = 0.05$. The maximum cyclic stresses applied to CP and MD laminates were, respectively, σ_x = 50, 60, 70, 80 MPa and σ_x = 105, 115, 125, 135 MPa. At least two specimens were tested for each load level. The test frequency was 10 Hz for CP laminates and 4 Hz for MD laminates to avoid over-heating.

All the specimens had a gage length of 120 mm. An observation region with a length of 60 mm across the specimen mid-section was considered for characterising the damage initiation and evolution. An axial extensometer MTS 632.29 F-30 with a calibrated length of 25 mm was mounted below the observation region to monitor the laminate stiffness throughout its fatigue life. The damage evolution, consisting of the initiation and propagation of multiple cracks in the off-axis plies, was monitored with a linear camera (Basler raL4096-24gm) mounted on a rail in front of the specimen and connected to the testing machine. To help the crack detection, a series of white LED was mounted behind the specimen, exploiting the transparency of the glass/epoxy system. Cracks were automatically detected using an in-house developed tool based on Gabor filter (see also [18, 24]).

3. Experimental results

3.1. Elastic properties and ply stresses

In composite laminates, the crack density evolution during cyclic loadings depends on the stresses acting on the off-axis plies (σ_1, σ_2, σ_6) rather than the remote ones (σ_x, σ_y, τ_{xy}). Given the remote loads, the ply stresses can be easily estimated with the Classical Lamination Theory (CLT), once the elastic and thermal properties of the individual plies are provided. Such properties were calculated from those of the fibre and matrix by means of classic micromechanics formulas accounting for the relevant fibre volume fraction V_f, and. The fibre and matrix properties, and the single ply properties are included as the supplementary material, along with the estimated laminate elastic moduli, which resulted to be in good agreement with the measured values.

It is important to highlight that while the mechanical stresses depend on the entity of the remote mechanical loads, the thermal contribution to the ply stresses is constant, and it is in general different among the three in-plane stress components (σ_1, σ_2, σ_6). Therefore, if we define the *local load ratios* in a ply as $R_{\sigma 1} = \sigma_{1,\min}/\sigma_{1,\max}$, $R_{\sigma 2} = \sigma_{2,\min}/\sigma_{2,\max}$, $R_{\sigma 6} = \sigma_{6,\min}/\sigma_{6,\max}$, and the biaxiality ratio as $\lambda_{12} = \sigma_6/\sigma_2$, we have that, in general:

1. the local load ratios vary in the same ply for different mechanical load levels;
2. the local load ratios vary in the same ply also for the three stress components;
3. the biaxiality ratio varies among the mechanical load levels and also between the maximum and minimum cyclic loads within the same load level ($\lambda_{12,\max} \neq \lambda_{12,\min}$).

However, for the produced laminates, considering a room temperature of 25 °C, CLT calculations showed that such variations were found to be negligible ($R_{\sigma1,CP} = 0.65 \div 0.80$, $R_{\sigma2,CP} = 0.26 \div 0.35$, $R_{\sigma1,MD} = -0.31 \div -0.48$, $R_{\sigma2,MD} = 0.29 \div 0.34$, $R_{\sigma6,MD} = 0.09 \div 0.10$, $\lambda_{12,max,MD} = 0.82 \div 0.88$, $\lambda_{12,min,MD} = 0.24 \div 0.26$). Accordingly, the local multiaxial stress state and load ratios the be considered very similar for laminates with the same stacking sequence, allowing a comparison of their fatigue behaviour.

3.2. Fatigue test results

In this section, the fatigue test results are reported, separately for cross-ply ($[0/90_2]_S$, CP) and multidirectional ($[0/50_2/0/\text{-}50_2]_S$, MD) laminates. For both stacking sequences, the influence of the microstructure is discussed on the life to crack initiation, crack propagation rate, crack density evolution, and stiffness degradation. Before presenting the experimental results, some considerations, calculations, and definitions valid for both the stacking sequences are made.

i. For the life to crack initiation, S-N curves were drawn considering the first six visible cracks in each specimen, as they were sufficiently far from each other to be regarded as independent events (see also [18,25,26]). All the S-N curves were fitted by a power-law, $\sigma_{max} = K \cdot N^a$. For all the S-N curves, also the lines referring to the 10% and 90% Probabilities of Survival (PS) are reported. The experimental scatter is then quantified by the scatter index T_σ, defined as the ratio between the stress corresponding to a PS of 10% and that corresponding to a PS of 90%, $T_\sigma = \sigma_{PS10}/\sigma_{PS90}$.
ii. The crack propagation is analysed by correlating the Crack Growth Rate (CGR) the Energy Release Rate (ERR, or G). The CGR can be measured by tracking the length of a crack sufficiently far from the others as a function of the number of cycles. When the crack is longer than about twice the ply thickness, it is in a steady state condition and its length increases almost linearly with the number of cycles, as supported by the approximately constant ERR of off-axis cracks propagating in the fibre direction [25,27] The CGR is then the slope of the crack length-versus-number of cycles curve, which can be measured experimentally. The ERR was calculated with the method proposed in [28], carrying out Finite Element (FE) analyses on Representative Volume Elements (RVEs) of a cracked laminate. A room temperature of 25 °C was considered to calculate the crack opening and sliding due to thermal loads. Due to the presence of thermal stresses, the Mode Mixity $MM = G_{II}/(G_I+G_{II})$ in MD laminates varies with remote mechanical load levels, as for the biaxiality ratio λ_{12}. Nonetheless, such a variation is small ($MM = 0.48 \div 0.57$), allowing a comparison between the two MD laminates to be made. The CGR is here reported as a function of the total ERR $G_{tot} = G_I + G_{II}$. For the cracks in the 90° ply of CP laminates, clearly, $G_{tot} = G_I$ as cracks propagate under pure Mode I condition ($MM = 0$).

All the Crack Growth Rate (CGR) versus Energy Release Rate (ERR, or G) curves are fitted by a power law, $CGR = C \cdot G_{tot,max}^{d}$.

i. The progressive fatigue damage evolution, consisting of the initiation and propagation of multiple cracks in the off-axis plies, was described by the *weighted* crack density, defined as [25]:

$$\rho_w = \frac{\sum_{i=1}^{n_c} c_i}{w \cdot L} \quad (1)$$

where c_i is the length of the ith crack, n_c the total number of cracks, and w and L the width and length of the observation region, respectively. Such a definition of crack density is indeed recommended to relate the damage scenario to the stiffness loss [25].

i. For comparison purposes the stiffness degradation is reported in all the plots as normalized to the initial value (see supplementary material). The elastic modulus was measured during the cyclic loads as the secant slope of the hysteresis cycles.

3.2.1. Cross ply (CP) laminates

Figure 4 shows the fatigue curves for first crack initiation of the CP laminates, in terms of the remote mechanical stress, σ_x, and the transverse stress acting on the 90° ply, σ_2. In general, different scatter bands in terms of σ_x are associated to different CP laminates, even if those for CP1 and CP2 are quite overlapped (Figure 4(a)). When plotted in terms of σ_2, a parameter that is better related to the crack formation process, thus allowing a more meaningful comparison, the relative positions between the three curves change. In this case, those for laminates CP1 and CP3 appear to fall within the same scatter band, while slightly longer lives characterise

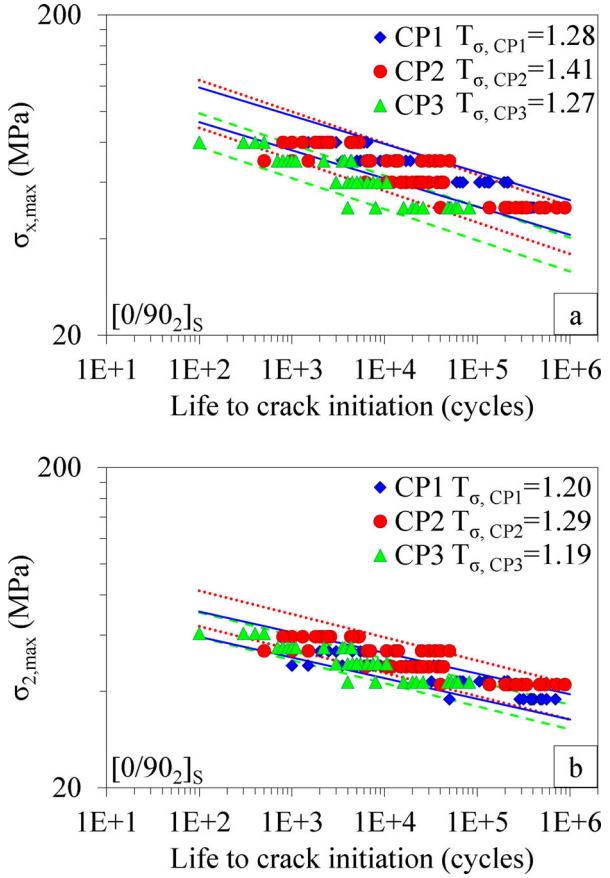

Figure 4. Life to crack initiation in the 90° ply of CP laminates ($[0/90_2]_S$) in terms of (a) remote mechanical stress, $\sigma_{x,max}$ and (b) transverse stress in the 90° ply, $\sigma_{2,max}$. Lines indicate the 90% and 10% Probabilities of Survival (PS); $T_\sigma = \sigma_{PS10}/\sigma_{PS90}$.

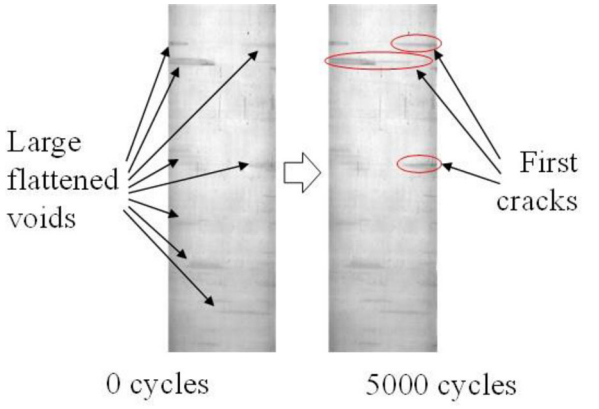

Figure 5. Effect of large, flattened voids of laminate CP1 on the initiation of the first cracks ($\sigma_{x,max}$ = 70 MPa).

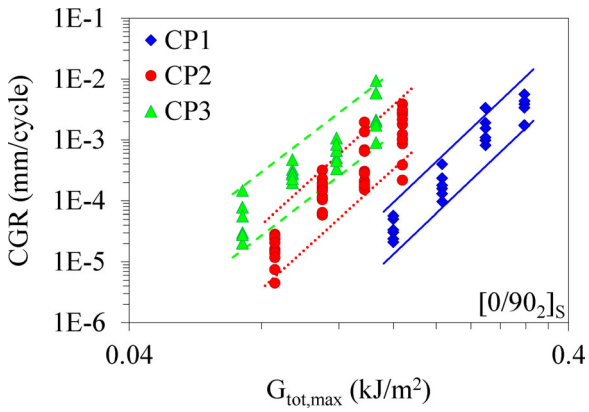

Figure 6. CGR versus ERR in the 90° ply of CP laminates ($[0/90_2]_S$) and 90–10% scatter bands.

laminate CP2 (Figure 4(b)). The shift of the curve towards shorter number of cycles of CP3 compared to CP2 is expected given the higher void content in the former. Even laminate CP1 is characterised by shorter lives to first crack initiation compared to laminate CP2 despite the smaller global void content and average void size (Table 1). This could be explained by the presence of large, flattened voids in laminate CP1, that considerably reduce the net section of the 90° ply. The majority of the first cracks in laminate CP1 were indeed observed to initiate in correspondence of such voids, for all the load levels (Figure 5).

The slope of the S-N curve does not seem to be significantly affected by the different microstructure, as also reported in [18]. The fatigue curve parameters are provided as supplementary material.

The Crack Growth Rate (CGR) versus the maximum total Energy Release Rate ($G_{tot,max}$) curves for CP laminates are shown in Figure 6, and the curve parameters are provided as supplementary material. A strong influence of the microstructure, intended as the combination of V_f and void content, can be observed. Compared to laminate CP2, laminate CP3 is characterised by a faster crack propagation, which is in line with the larger void content. On the other hand, cracks tend to propagate slower for laminate CP1, which is consistent with the significantly higher amount of resin, that could lead to a larger energy-dissipating process zone ahead of crack tips, and with the discontinuous void size distribution, that causes cracks to propagate in regions with less voids as the large ones are few and have already given their contribution to damage by promoting crack initiation. As for the S-N curves for first crack initiation, and as highlighted in [18], the slope of the curves does not appear to significantly change with different microstructural features.

Figure 7 shows the weighted crack density evolution and the stiffness degradation of the three CP laminates under a remote mechanical stress $\sigma_{x,max}$ = 80 MPa. The trends for other load levels are qualitatively similar and are provided as supplementary material. Damage (Figure 7(a)) evolves faster for laminate CP3 compared to CP2, as expected due to the similar V_f but higher void content for laminate CP3, and also suggested by the relevant S-N and CGR-ERR curves. The trends for laminate CP1 are similar to that of laminate CP2 at the beginning, in line with the relevant S-N curves for first crack initiation in terms of σ_x. Then, for laminate CP1 the

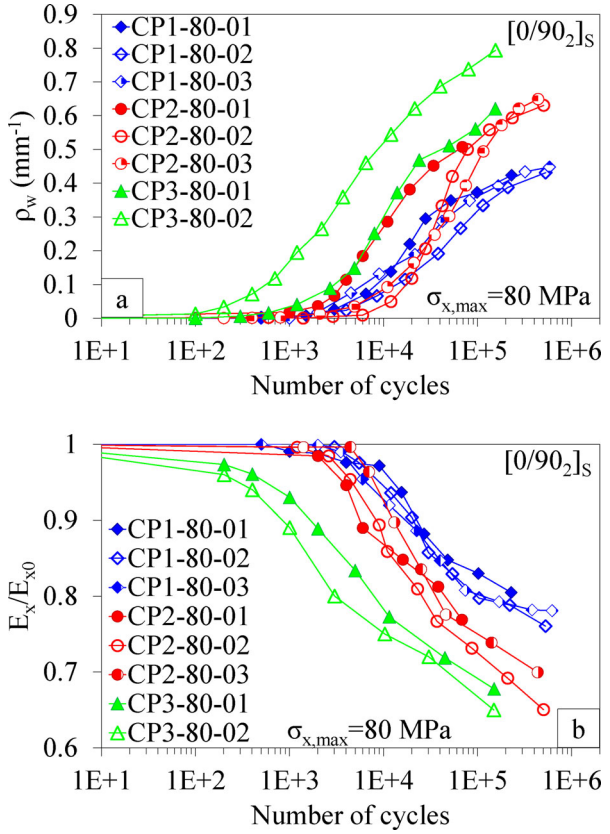

Figure 7. (a) Weighted crack density evolution, and (b) Stiffness degradation in CP laminates subjected to $\sigma_{x,max}$ = 80 MPa.

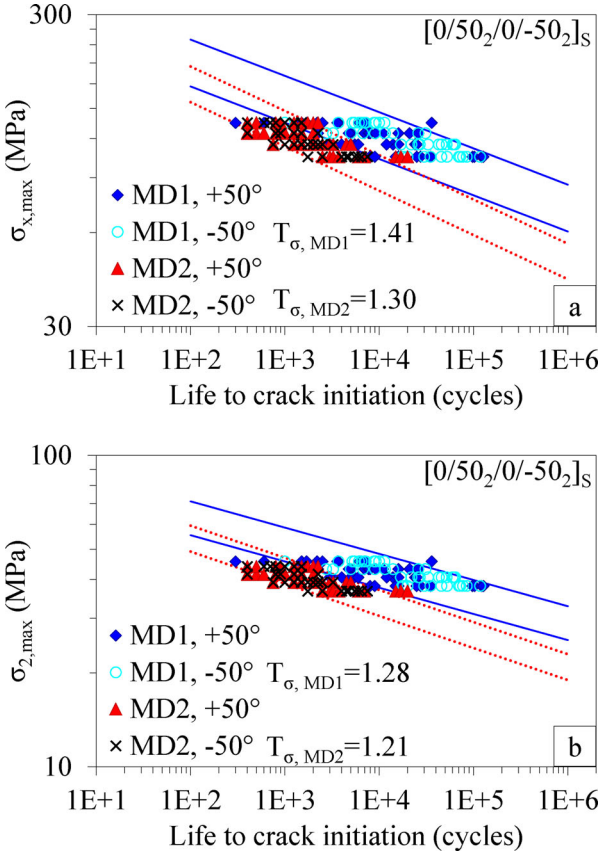

Figure 8. Life to crack initiation in the ±50° plies of MD laminates ([0/50$_2$/0/-50$_2$]$_S$) in terms of a) remote mechanical stress, $\sigma_{x,max}$, and b) transverse stress in the ±50° plies, $\sigma_{2,max}$. Lines indicate the 90% and 10% Probabilities of Survival (PS); T_σ=$\sigma_{PS10}/\sigma_{PS90}$.

damage evolves slower and approaches a smaller saturation level. Such a behaviour can be explained by the following considerations. First, as discussed above, although laminate CP1 has a lower A_v than laminate CP2, it is characterised by the presence of few very large voids, that were clearly involved in the initiation of the first cracks. As the total number of such large voids in laminate CP1 is small, they only affect the crack density evolution in the first stages. Then, the crack density progression is affected by voids of smaller size (Figure 3(a)), hence its evolution rate quickly decreases. In addition, laminate CP1 is also characterised by a much larger thickness, which reduces the crack density saturation level [29].

The stiffness drop (Figure 7(b)) clearly follows the opposite trend of the crack density evolution. Interestingly, the laminates with larger V_f are characterised by a premature stiffness drop due to the larger void contents compared to laminate CP1. It must be reminded, however, that in Figure 7b the stiffness is normalized to that of the pristine (undamaged) specimens, and that the initial elastic modulus was significantly higher for laminates CP3 and CP2 compared to CP1 (see supplementary material). So, for instance, after $1{\cdot}10^5$ cycles under σ_x = 80 MPa, $E_{x,CP1} \approx$ 14400 MPa, $E_{x,CP2} \approx$ 20500 MPa, $E_{x,CP3} \approx$ 20100 MPa.

3.2.2. Multidirectional (MD) laminates

The fatigue curves for first crack initiation of MD laminates are shown in Figure 8, in terms of remote mechanical stress σ_x and transverse stress acting on the ±50° plies σ_2. The clearer separation of the two curves of MD laminates in comparison to those of CP laminates can be attributed to the large difference in void content for the former stacking sequence. The S-N curves for the +50° and −50° plies are found to be reasonably overlapped, as expected given the same stresses and microstructures in those plies. The parameters of the S-N curves are provided as supplementary material.

Figure 9 shows the Crack Growth Rate (CGR) versus maximum total Energy Release Rate ($G_{tot,max}$) curves for MD laminates, whose parameters are provided as the supplementary material. The data for cracks in the +50° and −50° plies fall within the same scatter band for the individual laminates, as expected. Only a slight increase in the Crack Growth Rate can be observed in the presence of a much larger void content (laminate MD2), indicating a smaller effect of the microstructure on the crack propagation in the presence of relatively high shear stresses compared to the pure transverse stress

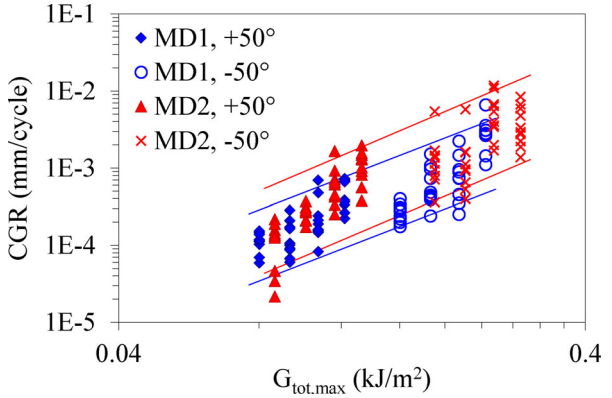

Figure 9. CGR versus ERR in the ±50° plies of MD laminates ([0/50$_2$/0/-50$_2$]$_S$) and 90–10% scatter bands.

condition of the cross-plies, in line with the findings of Maragoni et al. [18].

Figure 10 shows the trend of the weighted crack density and the stiffness decrease of MD laminates for a remote mechanical stresses $\sigma_{x,max} = 135$ MPa. The trends for the other load levels are qualitatively similar and are provided as supplementary material. As expected from the S-N and CGR-ERR curves, laminate MD2, characterised by a larger void content, exhibits an earlier crack density increase (Figure 10(a)), although tending to a similar saturation level for high number of cycles. For both laminates, the larger thickness of the −50° ply causes a faster damage evolution compared to the +50° ply due to a higher ERR, and at the same time a smaller saturation level, as expected [25]. As for CP laminates, the stiffness trends (Figure 10(b)) reflect those of the weighted crack densities, with an initially larger drop for the laminate with higher void content (MD2) and a comparable final stiffness decrease given the similar crack density saturation levels.

As reported in [18], also the present experimental data show a larger sensitivity to voids in LHS-rather than LMPS-dominated plies. Indeed, for laminates having similar V_f, the increase in damage evolution rate for MD laminates going from $A_v = 0.37\%$ (MD1) to $A_v = 4.2\%$ (MD2) is comparable to that obtained in CP laminates when going from $A_v = 0.73\%$ (CP2) to just $A_v = 1.48\%$ (CP3).

4. Prediction of first cracks initiation

In a recent work [20], the authors extended a previous criterion to predict the life to crack initiation [22] to account for the actual composite microstructure. The criterion proposes, as the driving force to fatigue crack initiation, the average value of the LHS or LMPS in a control volume V_c of the matrix, calculated by Finite Element (FE) analyses on micro-scale Representative Volume Elements (RVEs) capable of including voids. Such values of LHS and LMPS are referred to as LHS* and LMPS*. The

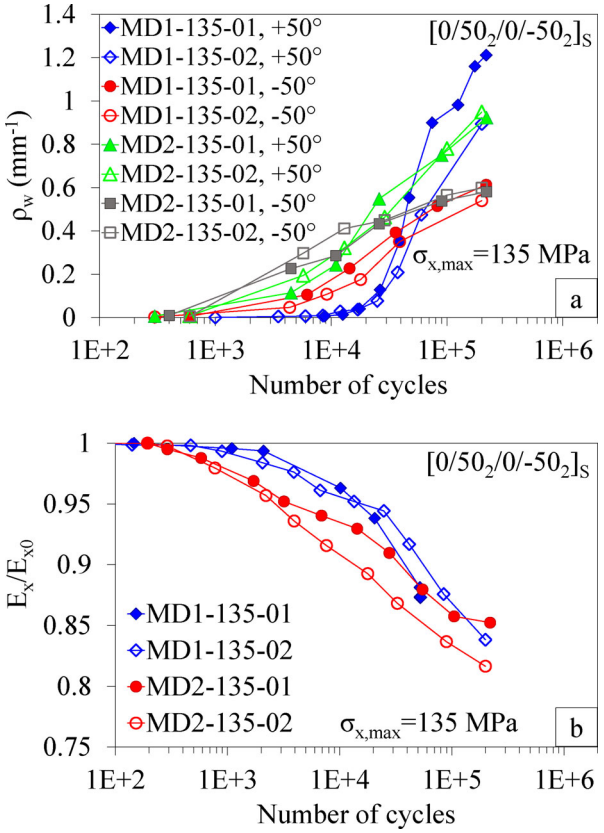

Figure 10. (a) Weighted crack density evolution, and (b) Stiffness degradation in MD laminates subjected to $\sigma_{x,max} = 135$ MPa.

control volume corresponds to a certain percentage of the matrix subjected to the highest LHS or LMPS values. As discussed in [20], this should be taken within the range 1%÷10%, as this corresponds to the matrix regions confined between closely packed fibres, where the micro-scale damage takes place, thus leading to the formation of an off-axis crack. The use of LHS* or LMPS* depend on the biaxiality ratio within the ply, λ_{12}, as mentioned in section 2.1. The reader is referred to Maragoni et al. [20] for a more comprehensive description.

To apply the criterion to the present experimental data, micro-scale material RVEs were first built. Using the experimental fibre diameter distribution and fibre volume fraction, fibres were initially placed in a regular pattern within a 2 D square and then "shaken" following the algorithm illustrated in [30]. A circular void of size equal to the experimental average equivalent void diameter was placed at the centre of the RVEs, the external dimensions of which were calculated to match the measured global void content [20]. Then, FE analyses were carried out on the RVEs applying individually the in-plane stress components acting on the ply (σ_1, σ_2, σ_6), calculated by means of Classical Lamination Theory (CLT). Then, the actual stress state in the off-axis plies was obtained by applying the superposition principle. In the FE analyses, periodic boundary

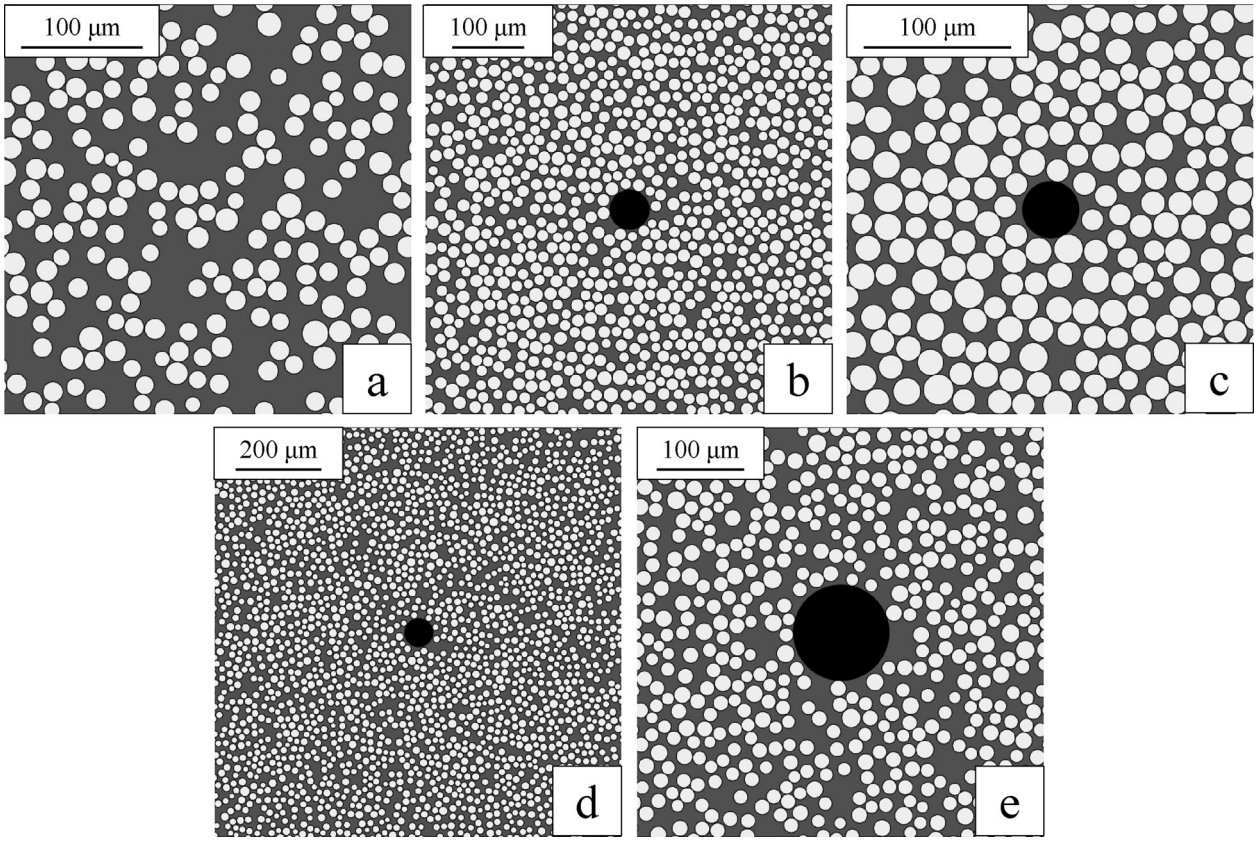

Figure 11. Representative Volume Elements (RVEs) of the produced laminates: (a) CP1, (b) CP2, (c) CP3, (d) MD1, and (e) MD2.

conditions were applied [30], thus reproducing a uniform void distribution, as that found in laminates CP2, CP3, MD1 and MD2.

A slightly different approach was used for laminate CP1, characterised by the presence of large, flattened voids clearly involved in the formation of the first fatigue cracks. To account for this kind of microstructure, periodic void-free RVEs were built, and the ply stresses relevant to the net section of the ply in correspondence of those large voids (about 4/5 of the 90° ply thickness) were applied in the FE analyses. This choice is believed to be reasonable as, given the flattened void shape and the load direction, the stress concentration factor due to the void itself is expected to be negligible, so that the effect of voids can be ascribed to a restriction of the net section of the transverse layer. Examples of RVEs for all the laminates are shown in Figure 11.

Once the FE analyses were carried out, LHS* and LMPS* were calculated for each laminate as indicated in [20], by averaging the LHS and LMPS values in the most critical matrix regions, referred to as the control volume V_c. In the RVEs containing voids, only the matrix volume belonging to the section containing the void was considered for the calculation of LHS* and LMPS*. This implicitly assumes that the crack forms in that section, due to the presence of the void itself, as confirmed by experimental observations.

Given the irregular fibre distribution, multiple RVEs were generated to represent each laminate, until a convergence on the LHS* and LMPS* was reached. In particular, 5, 9, and 13 RVEs were analysed for laminates CP1, CP2, and CP3, respectively, while 5 and 11 RVEs for laminates MD1 and MD2. The ply stresses, applied to the RVEs, were calculated with the Classical Lamination Theory (CLT), considering a room temperature of 25 °C.

As for the local load ratios for the ply stresses discussed in Section 3.1, also those for LHS* and LMPS* were found not to significantly vary with the remote mechanical load level for laminates with the same lay-up ($R_{LHS^*} = LHS^*_{min}/LHS^*_{max} = 0.28 \div 0.51$ for CP laminates, $R_{LMPS^*} = LMPS^*_{min}/LMPS^*_{max} = 0.16 \div 0.27$ for MD laminates), thus allowing the criterion proposed in [20] to be applied.

Figure 12 shows the S-N curves for first crack initiation in CP and MD laminates in terms of the proposed driving forces (LHS_{max}* and $LMPS_{max}$* for CP and MD laminates, respectively), calculated in a control volume $V_c = 5\%$. Similar results are found for other V_c values and are provided as supplementary material, highlighting once again the robustness of the proposed model with respect to the control volume choice. In the same figure, the 90%-10% scatter bands are reported, together with the scatter index T_σ, calculated considering all the data within a plot as a single series.

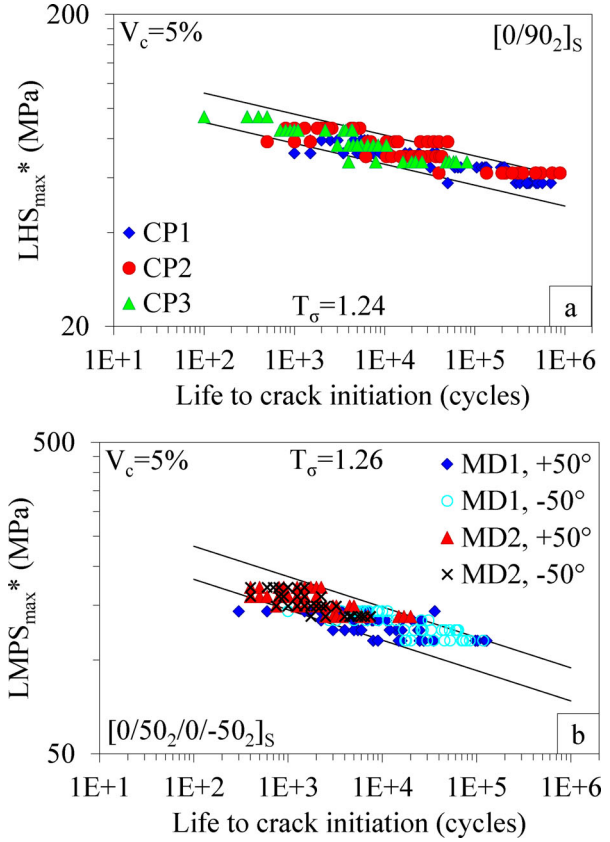

Figure 12. Life to crack initiation a) in terms of LHS* in the 90° plies of CP laminates ($[0/90_2]_S$), and b) in terms of LMPS* in the ±50° plies of MD laminates ($[0/50_2/0/-50_2]_S$). Control volume V_c=5% for both laminates. Lines indicate the 90% and 10% Probabilities of Survival (PS); $T_\sigma=\sigma_{PS10}/\sigma_{PS90}$.

It is possible to notice that for both stacking sequences the data fall well within the same scatter band. This is particularly evident for the MD laminates, whose curves were clearly apart from each other in terms of $\sigma_{2,max}$, and can be appreciated also for the cross-plies, whose curves in terms of $\sigma_{2,max}$ were already reasonably close. This further validates the capability of the predictive model proposed in [20] to account for variations in fibre volume fractions and void content, once proper micro-scale RVEs are built. Also, the model predictions appear to hold valid for microstructures obtained in both infused [20] and autoclave moulded composites, and even in the presence of thermal stresses, always present in the latter manufacturing process.

5. Conclusions

Three cross-ply ($[0/90_2]_S$), and two multidirectional ($[0/50_2/0/-50_2]_S$) laminates were manufactured by autoclave moulding, using different process parameters. The manufacturing settings were found to deeply affect the laminate microstructure in terms of fibre volume fraction, global void content, and average void size. For both stacking sequences, in the presence of a similar fibre volume fractions, larger void contents were found to promote the crack initiation and propagation, leading to an earlier rise in the crack density evolution and associated stiffness decrease. In cross-ply laminates, also, the combination of low fibre volume fraction with the presence of few large, flattened voids led to a reduced life to first crack initiation but also to a slower crack propagation. In addition, once cracks are formed in correspondence of the largest and most critical voids, the increase in crack density and the correlated stiffness drop evolved at a slower rate, as further cracking occurs in regions characterised by a significantly smaller void content and size. This highlights the need to account not only for global void content and average void size, but also to void size distribution and void spatial distribution.

From a qualitative point of view, the experimental results are in line with those found for vacuum infused laminates. It is remarked, however, that the present results could not be simply foreseen a priori from previous results, and that the present experimental campaign was needed to assess quantitatively the effect of the microstructure on autoclave-moulded laminates.

The combined effect of the fibre volume fraction, void content and void size on the fatigue damage initiation and evolution highlights the need to properly account for the local microstructure for an advanced and cost-effective design of composite parts. In this direction, a criterion recently proposed by the authors to predict the fatigue crack initiation in the presence of manufacturing-induced voids was applied to the experimental data, proving its capability to account for the simultaneous influence of both fibre volume fraction and void content, including the presence of large flattened voids and thermal stresses due to the manufacturing process (all conditions under which the model was not previously verified), thus improving the confidence in its general validity.

Acknowledgements

The authors wish to acknowledge the support and the computational resources made available by the High Performance Computing Lab at the Department of Management and Engineering (DTG), co-funded by the University of Padova in the framework of the program "Scientific research instrumentation 2015."

Disclosure statement

No potential conflict of interest was reported by the author(s).

Funding

The financial support received from the project "QUAR_SID19_01 - Effect of manufacturing-induced defects on the fatigue response of advanced composite

materials" by the University of Padova and Università degli Studi di Padova is also acknowledged.

References

1. Dill CW, Tipton SM, Glaessge EH, et al. Fatigue strength reduction imposed by porosity in a fiberglass composite. In: Masters, JE. editor. Damage detection in composite materials, ASTM STP 1128. Philadelphia: American Society for Testing and Materials; 1992. p. 152–162.
2. de Almeida SFM, Neto ZSN. Effect of void content on the strength of composite laminates. Compos Struct. 1994;28(2):139–148.
3. Olivier P, Cottu JP, Ferret B. Effects of cure cycle pressure and voids on some mechanical properties of carbon/epoxy laminates. Compos. 1995;26(7): 509–515.
4. Varna J, Joffe R, Berglund LA, et al. Effect of voids on failure mechanisms in RTM laminates. Compos Sci Technol. 1995;53(2):241–249.
5. Wisnom MR, Reynolds T, Gwilliam N. Reduction in interlaminar shear strength by discrete and distributed voids. Compos Sci Technol. 1996;56(1): 93–101.
6. Bureau MN, Denault J. Fatigue resistance of continuous glass fiber-polypropylene composites consolidation dependence. Compos Sci Technol. 2004; 64(12):1785–1794.
7. Hagstrand PO, Bonjour F, Manson JAE. The influence of void content on the structural flexural performance of unidirectional glass fibre reinforced polypropylene composites. Compos Part A. 2005; 36(5):705–714.
8. Chambers AR, Earl JS, Squires CA, et al. The effect of voids on the flexural fatigue performance of unidirectional carbon fibre composites developed for wind turbine applications. Int J Fatigue. 2006; 28(10):1389–1398.
9. Liu L, Zhang BM, Wang DF, et al. Effects of cure cycles on void content and mechanical properties of composite laminates. Compos Struct. 2006;73(3): 303–309.
10. Lambert J, Chambers AR, Sinclair I, et al. 3D damage characterization and the role of voids in the fatigue of wind turbine blade materials. Compos Sci Technol. 2012;72(2):337–343.
11. Schmidt F, Rheinfurt M, Horst P, et al. Multiaxial fatigue behaviour of GFRP with evenly distributed or accumulated voids monitored by various NDT methodologies. Int J Fatigue. 2012;43:207–216.
12. Huang Y, Varna J, Talreja R. Statistical methodology for assessing manufacturing quality related to transverse cracking in cross-ply laminates. Compos Sci Technol. 2014;95:100–106.
13. Scott AE, Sinclair I, Spearing SM, et al. Influence of voids on damage mechanisms in carbon/epoxy composites determined via high resolution computed tomography. Compos Sci Technol. 2014;90: 147–153.
14. Carraro PA, Maragoni L, Quaresimin M. Influence of manufacturing-induced defects on damage initiation and propagation in carbon/epoxy NCF laminates. Adv Manuf Polym Compos Sci. 2015;1(1): 44–53.
15. Protz R, Kosmann N, Gude M, et al. Voids and their effect on the strain rate dependent material properties and fatigue behaviour of non-crimp fabric composites materials. Compos Part B. 2015; 83(346/351):346–351.
16. Sisodia SM, Gamstedt EK, Edgren F, et al. Effects of voids on quasi-static and tension fatigue behaviour of carbon-fibre composite laminates. J Compos Mater. 2015;49(17):2137–2148.
17. Maragoni L, Carraro PA, Quaresimin M. Effect of voids on the crack formation in $[45/\text{-}45/0]_S$ laminate under cyclic axial tension. Compos Part A. 2016;91:493–500.
18. Maragoni L, Carraro PA, Peron M, et al. Fatigue behaviour of glass/epoxy laminates in the presence of voids. Int J Fatigue. 2017;95:18–28.
19. Mehdikhani M, Steensel E, Standaert A, et al. Multi-scale digital image correlation for detection and quantification of matrix cracks in carbon fiber composite laminates in the absence and presence of voids controlled by the cure cycle. Compos Part B. 2018;154:138–147.
20. Maragoni L, Carraro PA, Quaresimin M. Prediction of fatigue life to crack initiation in unidirectional plies containing voids. Compos Part A. 2019;127: 105638.
21. Mehdikhani M, Gorbatikh L, Verpoest I, et al. Voids in fiber-reinforced polymer composites: a review on their formation, characteristics, and effects on mechanical performance. J Compos Mater. 2019;53(12):1579–1669.
22. Carraro PA, Quaresimin M. A damage based model for crack initiation in unidirectional composites under multiaxial cyclic loading. Compos Sci Technol. 2014;99:154–163.
23. Quaresimin M, Carraro PA, Maragoni L. Early stage damage in off-axis plies under fatigue loading. Compos Sci Technol. 2016;128:147–154.
24. Glud JA, Dulieu-Barton JM, Thomsen OT, et al. Automated counting of off- axis tunnelling cracks using digital image processing. Comp Sci Technol. 2016;125:80–89.
25. Quaresimin M, Carraro PA, Mikkelsen LP, et al. Damage evolution under internal and external multiaxial cyclic stress state: a comparative analysis. Compos Part B. 2014;61:282–290.
26. Glud JA, Dulieu-Barton JM, Thomsen OT, et al. Fatigue damage evolution in GFRP laminates with constrained off-axis plies. Compos Part A. 2017;95: 359–369.
27. Ho S, Suo Z. Tunneling cracks in constrained layers. J Appl Mech. 1993;60(4):890–894.
28. Maragoni L, Carraro PA, Quaresimin M. Periodic boundary conditions for FE analyses of a representative volume element for composite laminates with one cracked ply and delaminations. Compos Struct. 2018;201:932–941.
29. Carraro PA, Maragoni L, Quaresimin M. Characterisation and analysis of transverse crack-induced delamination in cross-ply composite laminates under fatigue loadings. Int J Fatigue. 2019; 129:105217.
30. Maragoni L, Carraro PA, Quaresimin M. Development, validation, and analysis of an efficient micro-scale representative volume element for unidirectional composites. Compos Part A. 2018;110: 268–283.